

## A numerical study of the role of the vertical structure of vorticity during tropical cyclone genesis

To cite this article: T N Venkatesh and Joseph Mathew 2010 *Fluid Dyn. Res.* **42** 045506

View the [article online](#) for updates and enhancements.

### You may also like

- [Experimental study of a neutralizer-free gridded ion thruster using radio-frequency self-bias effect](#)  
Zhi YANG, , Honghui GUO et al.
- [Role of initial coherence on entanglement dynamics of two qubit X states](#)  
Namitha C V and S V M Satyanarayana
- [Analytical model for electromagnetic radiation from a wakefield excited by intense short laser pulses in an unmagnetized plasma](#)  
Zi-Yu Chen, Shi Chen, Jia-Kun Dan et al.

# A numerical study of the role of the vertical structure of vorticity during tropical cyclone genesis

T N Venkatesh<sup>1</sup> and Joseph Mathew<sup>2</sup>

<sup>1</sup> Flosolver Unit, National Aerospace Laboratories, PO Box 1779, Bangalore 560017, India

<sup>2</sup> Department of Aerospace Engineering, Indian Institute of Science, Bangalore 560012, India

E-mail: [tnv@flosolver.nal.res.in](mailto:tnv@flosolver.nal.res.in) and [joseph@aero.iisc.ernet.in](mailto:joseph@aero.iisc.ernet.in)

Received 9 October 2008, in final form 20 January 2010

Published 20 April 2010

Online at [stacks.iop.org/FDR/42/045506](http://stacks.iop.org/FDR/42/045506)

Communicated by K Ishii

## Abstract

An eight-level axisymmetric model with simple parameterizations for clouds and the atmospheric boundary layer was developed to examine the evolution of vortices that are precursors to tropical cyclones. The effect of vertical distributions of vorticity, especially that arising from a merger of mid-level vortices, was studied by us to provide support for a new vortex-merger theory of tropical cyclone genesis. The basic model was validated with the analytical results available for the spin-down of axisymmetric vortices. With the inclusion of the cloud and boundary layer parameterizations, the evolution of deep vortices into hurricanes and the subsequent decay are simulated quite well. The effects of several parameters such as the initial vortex strength, radius of maximum winds, sea-surface temperature and latitude (Coriolis parameter) on the evolution were examined. A new finding is the manner in which mid-level vortices of the same strength decay and how, on simulated merger of these mid-level vortices, the resulting vortex amplifies to hurricane strength in a realistic time frame. The importance of sea-surface temperature on the evolution of full vortices was studied and explained. Also it was found that the strength of the surface vortex determines the time taken by the deep vortex to amplify to hurricane strength.

## 1. Introduction

Tropical cyclones (TC), also called hurricanes, are large three-dimensional vortices in the atmosphere. Computational models are very useful tools for studying these systems since direct controlled experiments are not possible and laboratory simulations are difficult. A wide variety of models of different resolution and sophistication are used for basic TC studies. These range from high-resolution general circulation models (GCM), the regional models such as MM5, RAMS and WRF and simple three-level models. With the availability

of increasing computing power, there is a natural tendency to use bigger models such as MM5/WRF. For example, Fudeyasu *et al* (2008) have successfully simulated the life cycle of tropical cyclones using the global, nonhydrostatic, cloud-system-resolving model NICAM at a horizontal resolution of 7 km. At the same time, the use of simpler three-layer models continues because they can throw light on important processes (Emanuel 1989, Zhu *et al* 2001, Zhu and Smith 2002). The aim is to retain the minimum number of relevant features to get a reasonable picture.

The present authors have proposed a model of TC genesis (Venkatesh 2003, Venkatesh and Mathew 2004) in which mesoscale mid-level vortices (termed MCV, for mesoscale convectively generated vortices) play a crucial role in the early stages. In this model, the early stages consist of mid level MCVs that interact. This process is largely two-dimensional and non-axisymmetric. The later stages consist of the larger merged vortex, which extends down to the boundary layer. We consider the initial evolution to be ‘top-down’ in a manner similar to that proposed by others (Bister and Emanuel 1997, Ritchie and Holland 1997). Subsequent development of the merged vortex takes place in an essentially axisymmetric manner. The other view of TC genesis is the ‘bottom-up’ approach suggested by Hendricks *et al* (2004) and Montgomery *et al* (2006). Interactions of mesoscale vortices prior to TC genesis have been observed in the Pacific (Ritchie and Holland 1997) and the Bay of Bengal (Venkatesh 2006). Some of the important issues that can be elucidated from numerical simulations are: (i) the difference in the evolution of mid-level MCVs and deep vortices, which extend down to the boundary layer, (ii) evolution of MCVs following merger and (iii) the effect a weak surface vortex has on mid-level vortices. The objective of this study is to answer these questions.

To simulate the essential features of this process, a multi-level model is required. Therefore, an eight-level, axisymmetric, balanced vortex model was developed. The main features of this model are that it solves the hydrostatic, balanced flow equations with simple parameterizations of the boundary layer and clouds. Also, the height is used as a coordinate instead of the pressure (or sigma) as is common in many atmospheric models. An advantage of using height is that the location and extent of the mid-level vortices can be specified exactly. The need to develop another simple hurricane model arose because most of the simple models that have been developed (Zhu *et al* 2001, Zhu and Smith 2002), including those available in the public domain (Emanuel 1995), have been three-layer models. In a three-layer model, the cloud parameterization is done in a very simple manner, keeping the essential physics required for studying certain effects. Such a model would not be appropriate for our study since we are interested in mid-level vortices and their extension to the boundary layer, as well as finite-amplitude effects. Therefore, a model with eight layers, which are sufficient to resolve the vertical structure, was developed. The model is similar to Sundqvist’s (1970) ten-level hurricane model, which has been used extensively by Challa and Pfeffer (1980) and Challa *et al* (1998) for many studies. The model of the boundary layer cumulus mass flux is similar to Emanuel’s model based on quasi-equilibrium.

The structure of the paper is as follows: formulation of the model equations is described in section 2. The numerics and computational details of the validation with semi-analytical results are provided in section 3. Section 4 contains the main results of the simulations we carried out. Studies with deep vortices, mid-level vortices and the parameter sweep experiments are described. Conclusions are presented in section 5.

## 2. Model formulation

As stated in the Introduction, three-layer models are not adequate for our study since we are interested in mid-level vortices and their extension to the boundary layer. To represent the

vertical structure, a sufficient number of layers, at least five, are required. The present model formulation can handle an arbitrary number of levels. However, to keep the model economical, eight levels are used.

To obtain a reasonable representation of the flow structure and physics, an axisymmetric, hydrostatic balanced vortex model is used with the effects of clouds, radiation, boundary layer and sea surface parameterized in a simple manner. The balanced vortex approximation was first used by Eliassen (1952) for the study of meridional circulations. It has since been used extensively in hurricane-related studies (Schubert and Hack 1982, 1983) and also for studies of idealized monsoon systems (Wirth 1998). The main assumptions are that the radial flow is in a state of gradient wind balance and that there is hydrostatic balance in the vertical. Together, they imply that the azimuthal velocity and temperature perturbations are related by the thermal wind equation. Also, the secondary flow in the vertical plane can be obtained by solving a generalized Poisson equation.

The domain was divided into the surface boundary layer and the outer region. The boundary layer was considered to be the sub-cloud layer and to have a constant depth  $h_{BL}$ . The outer region extended from the top of the boundary layer to a height  $z_{max}$ .

The prognostic equations in the interior are for the azimuthal velocity  $v$  and the saturation equivalent potential temperature  $\theta_e^*$  (which is nearly a conserved quantity).

$$\frac{\partial v}{\partial t} = -u\eta - w \frac{\partial v}{\partial z} + D_v, \quad (1)$$

$$\frac{\partial \theta_e^*}{\partial t} = -u \frac{\partial \theta_e^*}{\partial r} - w \frac{\partial \theta_e^*}{\partial z} + D_\theta + \dot{H}_{rad}. \quad (2)$$

Here  $u$  is the radial velocity,  $w$  the vertical velocity,  $D_v$  represents the diffusion of  $v$  (modelled),  $\eta = f + \zeta = f + v/r + \partial v/\partial r$  is the absolute vorticity,  $f$  is the Coriolis parameter due to the Earth's rotation,  $D_\theta$  represents the diffusion of  $\theta_e^*$  and  $\dot{H}_{rad}$  the radiative cooling term. In Sundqvist's model, specific humidity is used as the second prognostic variable. Using  $\theta_e^*$  instead has the advantage that explicit treatment of condensation is not required in the prognostic equations (heating due to the condensation term appears in the cloud model as will be described later). A mean value of the virtual potential temperature  $\bar{\theta}_v$  was defined, which is a function of  $z$  only. Perturbations of the virtual potential temperature ( $\theta_v = \theta[1 + 0.61q]$ ) from the mean value  $\bar{\theta}_v$  were related to  $v$  by the thermal wind equation

$$\frac{\bar{\theta}_v}{\bar{\rho}g} \frac{\partial}{\partial z} \left[ \frac{\bar{\rho}v^2}{r} + \bar{\rho}fv \right] = \frac{\partial \theta_v}{\partial r}. \quad (3)$$

Given  $v$ , this equation can be solved for  $\theta_v$ . An additional constraint is that the values of  $\theta_v$  should be less than  $\theta_v^*$  (the saturation value), which was calculated from  $\theta_e^*$  and the pressure  $p$ .

The perturbation pressure was obtained from the gradient wind relation

$$\frac{1}{\rho} \frac{\partial p}{\partial r} = \frac{v^2}{r} + fv. \quad (4)$$

The flow in the  $r$ - $z$  plane was obtained by solving a Poisson equation for the streamfunction  $\psi$

$$\frac{\partial}{\partial r} \left[ A \frac{\partial \psi}{\partial r} + B \frac{\partial \psi}{\partial z} \right] + \frac{\partial}{\partial z} \left[ C \frac{\partial \psi}{\partial r} + D \frac{\partial \psi}{\partial z} \right] = \frac{\partial S_q}{\partial r} + \frac{\partial S_f}{\partial z}, \quad (5)$$

where

$$A = -\frac{1}{r} \frac{g}{\bar{\theta}} \frac{\partial \bar{\theta}_v}{\partial z}, \quad B = \frac{1}{\bar{\rho} r} \frac{\partial}{\partial z} \left[ \frac{\bar{\rho} v^2}{r} + \bar{\rho} f v \right],$$

$$C = \left( \frac{2v}{r} + f \right) \frac{1}{r} \frac{\partial v}{\partial z},$$

$$D = -\left( \frac{2v}{r} + f \right) \frac{1}{r} \left( \frac{\partial v}{\partial r} + \frac{v}{r} + f \right),$$

$$S_q = \left( \frac{\bar{\rho} g \dot{Q}}{C_p \bar{T}} \right), \quad S_f = -\left( \frac{2v}{r} + f \right) D_v.$$

Boundary conditions for solving the  $\psi$  are needed at the lower, upper, inner and outer boundaries. They were prescribed as follows: (i) at  $r = 0$  and  $z = z_{\max}$ ,  $\psi = 0$ , (ii) in the lower domain, i.e. at  $z = h_{BL}$ ,  $\psi$  is calculated from the boundary layer model and (iii) at  $r = r_{\max}$ , extrapolation boundary conditions were used.

The velocity components  $u$  and  $w$  were obtained from the streamfunction:

$$u = \frac{1}{\bar{\rho} r} \frac{\partial \psi}{\partial z}, \quad w = -\frac{1}{\bar{\rho} r} \frac{\partial \psi}{\partial r}.$$

A detailed derivation of the above equation (5) can be found in appendix C of Venkatesh (2003).

Models are needed for the diffusion terms  $D_v$  and  $D_\theta$  and radiation  $\dot{H}_{\text{rad}}$  in equations (1) and (2), heating rate  $\dot{Q}$  in the source term  $S_q$  of equation (5), and  $\psi$  and  $\theta_v$  at the top of the boundary layer. The diffusion terms were obtained from the simple eddy viscosity model:

$$D_v = \frac{\partial}{\partial z} (\tau_{\phi z}) + \frac{1}{r^2} \frac{\partial}{\partial r} (r^2 \tau_{\phi r})$$

with

$$\tau_{\phi z} = K_V \frac{\partial v}{\partial z}, \quad \tau_{\phi r} = K_H \left( \frac{\partial v}{\partial r} - \frac{v}{r} \right)$$

and

$$D_\theta = \frac{\partial}{\partial z} \left( K_V \frac{\partial \theta_e^*}{\partial z} \right) + \frac{1}{r^2} \frac{\partial}{\partial r} \left( r^2 K_H \frac{\partial \theta_e^*}{\partial r} \right)$$

where  $K_H$  and  $K_V$ , the eddy diffusivities (assumed to be the same for both momentum and heat transfer), were calculated from the boundary layer model, and are functions of  $r$  and  $z$ . The radiation term

$$\dot{H}_{\text{rad}} = -\frac{\theta_e'}{\tau_{\text{rad}}}, \quad (6)$$

where  $\tau_{\text{rad}}$  is a decay time of the order of 24 h.

### 2.1. The boundary layer model

The boundary layer is modelled by a single layer in which the evolution equation solved for  $\theta_e$  is

$$\frac{\partial \theta_e}{\partial t} = -u \frac{\partial \theta_e}{\partial r} - w_m \frac{\partial \theta_e}{\partial z} + D_\theta + \dot{H}_{\text{rad}}. \quad (7)$$

The azimuthal velocity is assumed to decrease linearly from its value at the top of the boundary layer, to the top of the surface layer by 20% (Montgomery *et al* 2001). The radial inflow velocity  $u_{\text{BL}}$  is deduced in a manner similar to Ooyama (1969) and Emanuel (1986). In equation (1) for  $v$  in the boundary layer, the major balance is between the diffusion term and the radial advection term. So,

$$u_{\text{BL}} \eta = -\frac{C_D |v| v}{h_{\text{BL}}}.$$

In regions of strong convective activity, vertical velocity can become large and the vertical convection term is included. Otherwise the computed values of  $u$  can become unrealistic. Therefore, in cloud regions, the following expression is used.

$$u_{\text{BL}} \eta = -\frac{C_D |v| v}{h_{\text{BL}}} - w_{\text{BL}} \frac{\partial v}{\partial z}.$$

In the lower part of the boundary layer, the surface layer, Deacon's formula is used to calculate the aerodynamic drag coefficient

$$C_D = 1.1 \times 10^{-3} + 4.0 \times 10^{-5} V.$$

Here,  $V$  is the speed at the top of the surface layer (10 m) in metres per second. This formula is probably the most widely used one in models of this class (Montgomery *et al* 2001, Ooyama 1969).

Matching of the fluxes at the top of the boundary layer leads to estimates of the eddy diffusivities

$$K_{V_{\text{BL}}} = C_D * V / h_{\text{BL}},$$

$$K_{H_{\text{BL}}} = K_{V_{\text{BL}}} * (l_h / l_v)^2$$

with typical values of  $l_h$  and  $l_v$  being 2000 and 200, respectively. In the interior, the eddy viscosities decay with height  $z$  above the boundary layer value by a factor  $\exp(-a(z/z_{\text{max}})^2)$ . Values in the range 3–10 for the constant  $a$  did not cause any significant change to the results. Also, the minimum values of 1 for  $K_V$  and 100 for  $K_H$  were prescribed.

The streamfunction at the top of the boundary layer is required for the interior solution. It is the sum of two parts: the Ekman pumping component and the additional cumulus mass flux in regions of convection. The Ekman pumping component  $w_{\text{ca}}$ , also called the clear air component, results from the induced radial velocity  $u_{\text{BL}}$ . Therefore

$$\psi_{\text{Ekman}} = \rho_{\text{BL}} u_{\text{BL}} h_{\text{BL}}.$$

### 2.2. The cloud model

Clouds are very important constituents of the atmosphere and the most difficult to model. An accurate representation of clouds requires covering a range of scales from the microphysical to the mesoscale. There are various degrees of approximation from one-dimensional models

to those with full microphysics (Houze 1993). Since incorporation of such details would increase the complexity and be inappropriate in our model, we model only the primary effects of cumulus clouds.

The cloud model in this study consists of a boundary layer part and an interior part. Grid points where the Ekman pumping is upward ( $w > 0$ ) are considered to have deep cumulus clouds. In the boundary layer the cumulus mass flux is calculated by a formulation that is similar to Emanuel (1995). The equation for moist entropy in the boundary layer  $s_b = C_p \ln \theta_e$  is

$$\frac{d_h s_b}{dt} + (w_{ca} - \delta w_{cm})(s_m - s_b)/h_{BL} = \frac{C_D |\mathbf{V}_b| (k_s^* - k_b)}{T_b} + \dot{Q}_{rad}/T_b, \quad (8)$$

where  $\delta w_{cm}$  is the net cumulus updraft velocity (this is the difference between the updraft and downdraft velocities),  $V_b$  the surface layer velocity,  $k_b$  the moist enthalpy of the boundary layer,  $k_s^*$  the saturation moist enthalpy at the sea-surface,  $\dot{Q}_{rad}$  the radiative cooling term,  $T_b$  the boundary layer temperature,  $d_h/dt$  the horizontal derivative and  $s_m$  the entropy at the ‘middle’ level where downdrafts originate. The quasi-equilibrium assumption implies that the time derivative and the radiative cooling term are neglected. Then, the equilibrium cumulus updraft velocity

$$\delta w_{cmeq} = \frac{C_D |\mathbf{V}_b| (k_s^* - k_b)}{T_b} + w_{ca}. \quad (9)$$

The actual cumulus mass flux relaxes to this equilibrium value on a timescale  $\tau_{mc}$  that is of the order of a few hours.

$$\frac{\partial \delta w_{cm}}{\partial t} = \frac{\delta w_{cmeq} - \delta w_{cm}}{\tau_{mc}}. \quad (10)$$

In the interior, the local heating rate  $\dot{Q}$  is determined by calculating the difference between the ‘cloud temperature’ at that point and the local temperature. In terms of the model variables,

$$\dot{Q}(r, z) = \xi(\theta_v^C - \theta_v). \quad (11)$$

$\theta_v^C$  is the potential temperature of a parcel that is lifted moist adiabatically (keeping  $\theta_e^*$  constant) from the top of the subcloud layer. Therefore,  $\theta_v^C$  is equal to  $\theta_v^*$ , calculated from  $\theta_e^*$  at the lowest interior level and the local value of pressure. The parameter  $\xi$  is found for each column by equating the column integral of  $\dot{Q}$  to the enthalpy flux into the column from the boundary layer, which in turn is mainly the transfer from the sea surface. The enthalpy flux is modelled as

$$e_{flux} = \delta w_{mc} T_{BL} \frac{\Delta s}{h_{BL}},$$

where

$$\Delta s = \Delta(C_p \ln \theta_e) = C_p \frac{\Delta \theta_e}{\theta_e}$$

and  $\Delta \theta_e = \theta_{es}^* - \theta_{eBL}$ .

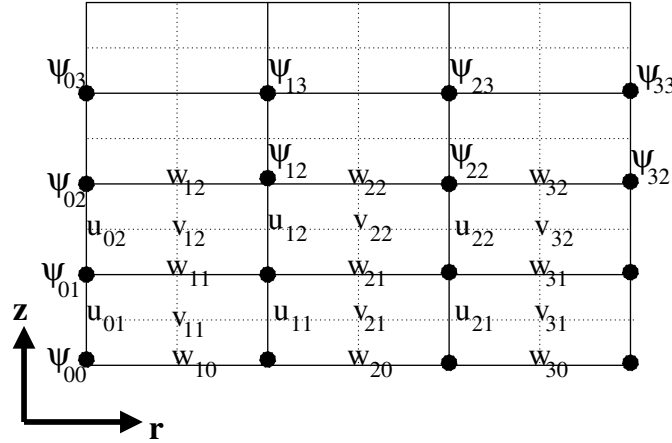


**Figure 1.** Schematic diagram of a portion of the staggered grid used for the computation. The azimuthal velocity ( $v$ ) is located at the cell centre, whereas the radial ( $u$ ) and vertical ( $w$ ) velocities are at the cell faces. The streamfunction  $\psi$  is located at the corners of a cell.

### 3. Numerics and simulation details

The domain of calculation is in the  $r$ - $z$  plane, bounded by  $r_{\max}$  and  $z_{\max}$ , respectively. The locations of the various quantities on the grid used are as shown in figure 1. In the staggered grid,  $\theta_e^*$ ,  $\theta_v$  and the other thermodynamic quantities are co-located with  $v$  at the cell centre, while  $u$  and  $w$  are at the cell faces and the streamfunction  $\psi$  is at the corners. The staggered grid used here is similar to the Arakawa C-grid. The advantage of using such a grid is that oscillations of pressure are suppressed. Moreover, application of the boundary conditions can be done exactly.

To start the calculation, initial fields of  $v$  and  $\theta_e^*$  have to be specified. The initial velocity field for a deep vortex was calculated using the following expression:

$$v(r, z) = \frac{2v_{\max}(r/r_{v_{\max}})}{1 + (r/r_{v_{\max}})^2} \left[ 1 - \frac{z}{z_{\max}} \right]. \tag{12}$$

For a Rankine vortex, the velocity increases linearly up to  $r_{v_{\max}}$  and then varies as  $1/r$ . This profile is a smoothed approximation since the velocity increases linearly for small  $r/r_{v_{\max}}$ , decreases as  $1/r$  for large  $r/r_{v_{\max}}$  and varies smoothly in between. The maximum value is  $v_{\max}$  at  $r_{v_{\max}}$ . The velocity field initialization for a mid-level vortex is described in section 4.4. The initial values of  $p$ ,  $\theta$  and  $\theta_e^*$  are from Jordan’s mean tropical sounding (Jordan 1958). Initial values of  $u$  and  $w$  are set to zero.

The sequence of computations in each time step is as follows:

1. The prognostics equations for  $v$  (equation (1)) and  $\theta_e^*$  (equation (2)) are integrated using a second-order time-stepping scheme. Details of the scheme are described below.
2. Pressure is calculated from the balance condition (equation (4)) and perturbation  $\theta_v$  from equation (3).
3. Various parameterized quantities (eddy diffusion terms, heating rates from the cloud and radiation models) are calculated in the interior. The source terms for the Poisson equation and the prognostic equations are thus obtained.

4. Integration of the boundary layer model is done to obtain the boundary conditions for the Poisson equation and the prognostic equations.
5. The Poisson equation for the streamfunction  $\psi$  (equation (5)) is solved using a standard iteration scheme.
6. The radial and vertical velocities are calculated from  $\psi$ .

In this sequence of calculations, steps 1 and 5 are most important. A mixed scheme (Kim and Moin 1985, Khalili *et al* 1997) of explicit time-stepping for nonlinear terms (denoted NL) and implicit time-stepping for diffusion terms was implemented for equation (1) as

$$\frac{v^{n+1} - v^n}{\Delta t} = -\frac{1}{2} (3NL^n - NL^{n-1}) + \frac{1}{2} (D_v^{n+1} + D_v^n). \quad (13)$$

Approximate factorization of the diffusion terms leads to the form

$$\left(I - \frac{\Delta t}{2} D_z\right) \left(I - \frac{\Delta t}{2} D_r\right) v^{n+1} = v^n - \frac{\Delta t}{2} (3NL^n - NL^{n-1}) + \frac{\Delta t}{2} (D_r + D_z) v^n, \quad (14)$$

where  $I$  is the identity operator, and terms of order  $(\Delta t)^2$  have been dropped. Then, inversion of tridiagonal matrices in each direction suffices. The prognostic equation for  $\theta_c^*$  (2) is treated similarly. A CFL condition for stability is

$$\Delta t = \frac{h_{BL} CFL}{V_{\max}}.$$

Here, CFL = 0.75 was used.

The Poisson equation for  $\psi$  was solved iteratively, with central differences used for evaluating the derivatives. For the other equations also, central differences are used for discretization.

The numerical parameters that can be varied in the model are given in table 1. In addition, there are flags for switching on the clouds and radiation and for specifying a full or mid-level vortex in the initial field. The main differences between Sundqvist's model and the present model are as follows. (i) The vertical coordinate  $z$  is used here instead of pressure, (ii) an evolution equation for  $\theta_c^*$  is used, not humidity  $q$  and (iii) the modelling of cloud heating is different.

### 3.1. Validation of the numerics: decay of a deep vortex

To test the dynamics and the numerics of the model/code, it was run with cloud terms switched off. Eliassen and Lystad (1977) studied a similar problem and arrived at an expression for the half-life based on a simplified theory. Montgomery *et al* (2001) have also used this expression to study the effect of drag parameterizations on the computed half-lives. The expression for the half-life is

$$t_{1/2} = \frac{H - h}{\xi^2 C_D V_{\text{initial}}},$$

where  $H$  is the height of the vortex,  $h$  the boundary layer height,  $C_D$  the drag coefficient,  $V_{\text{initial}}$  the maximum initial azimuthal velocity and  $\xi$  the reduction factor.

The computed and theoretical values of half-lives are listed in table 2. One can see that there is reasonable agreement with the theory. This is a validation of the basic numerics of the code and also the range of eddy viscosities chosen. The differences could be due to the fact that in the theory an assumption is that the flow evolves to a state of cyclostrophic balance.

**Table 1.** List of model and simulation parameters that can be varied in the code.

Parameter	Symbol	Units	Mean value (control)
Domain size: horizontal	$R_{\max}$	km	500
Domain size: vertical	$z_{\max}$	km	16.0
Boundary layer height	$h_{\text{BL}}$	km	1.0
Initial vortex strength	$v_{\max}$	$\text{m s}^{-1}$	11.0
Radius of maximum winds	$r_{v_{\max}}$	km	90.0
Sea-surface temperature (SST)	$T_{\text{sea}}$	K	300.5
Base latitude		deg	20
Vortex height		km	16.00
Radiation time constant	$\tau_{\text{rad}}$	h	24.0
Base latitude		deg	20.0
Cumulus mass flux time constant	$\tau_{\text{mc}}$	h	2.0
Base drag coefficient in Deacon's formula	$C_{\text{D0}}$	–	$1.1 \times 10^{-3}$
Velocity-dependent part of drag	$C_{\text{Dr}}$	$\text{s m}^{-1}$	$4.0 \times 10^{-5}$
Time step	$\Delta t$	min	5
Integration time	$t_{\text{max}}$	h	240
CFL number	CFL	–	0.75
Number of cells in the $r$ direction	$n_r$	–	50
Number of vertical layers	$n_z$	–	8

**Table 2.** Comparison of computed half-lives with the theory of Eliassen and Lystad for various initial vortex strengths, and with vortex heights ( $H$ ) of 5 and 10 km.

$V_{\text{initial}}$ ( $\text{m s}^{-1}$ )	$t_{1/2}$ (h)		
	Theory	Computed	
		$H = 5$ km	$H = 10$ km
10	115.0	101.70	111.32
20	46.0	48.60	50.31
30	25.0	28.00	28.95
50	11.0	11.83	12.94

The decay of the maximum velocity is algebraic in time. For  $V_0 = 10$  and 20, velocities decay at the same rate throughout and the velocity maximum is at the surface at all times. For stronger and deeper vortices ( $V_0 = 30, 50$ ;  $H = 10$  km), the vorticity near the surface decays at a slightly faster rate and the velocity maximum is lifted up. This indicates that the eddy viscosities are not sufficient in the later stages. However, since this happens after the velocity has reached a quarter of the initial value, we do not expect it to have a significant impact on other simulations.

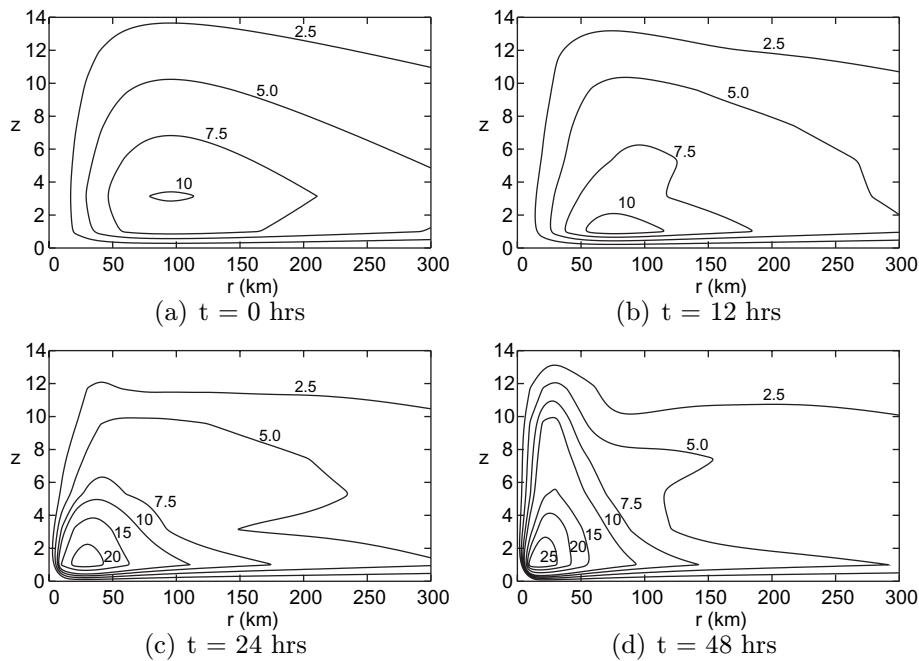
The computational costs of running this model are quite low. For example, a 10 day run with the full model (50 radial points and  $\Delta t$  of 5 min) takes 4 min of real time on a desktop system with a 3 GHz Intel Pentium IV processor and 1 GB of RAM.

#### 4. Studies with the full model

The studies with the full model were of deep vortices whose velocity maxima in the vertical were at the top of the boundary layer, and mid-level vortices whose velocity maxima were at level 3 or 4.

**Table 3.** List of experiments conducted with full vortices. The parameters changed and the values are listed.

Parameter	Units	Range
Initial vortex strength: $V_0$	$\text{m s}^{-1}$	2, 5, 8, 10, 11 and 12
Domain size: $R_{\text{max}}$	km	500, 1000
Radius of maximum winds	km	50, 60, 70, 80, 90, 100, 125, 150
$T_{\text{sea}}$	K	298.5–302.5 (in steps of 0.5)
Base latitude	deg	15, 16, 17, 18, 19, 20, 22.5, 25.0

**Figure 2.** Evolution of the vortex with an initial maximum velocity of  $11 \text{ m s}^{-1}$ . Azimuthal velocity contours are plotted at intervals of  $2.5 \text{ m s}^{-1}$ , starting from  $2.5$  until  $10 \text{ m s}^{-1}$  and at intervals of  $5 \text{ m s}^{-1}$  from  $10 \text{ m s}^{-1}$  onwards.

A number of parameter studies were conducted using the model. A list of them is given in table 3.

#### 4.1. Evolution of deep vortices

The behaviour of a deep vortex that extends from the top of the boundary layer to the top of the troposphere was studied by a series of simulations in which the cloud model was turned on. The initial vortex had maximum velocity at the top of the boundary layer and decreased linearly with height, reaching zero at  $z_{\text{max}}$ . The radial profile of azimuthal velocity was the same as that used for the decay studies (equation (12)). The mean initial profiles for  $\theta_v$ ,  $\bar{p}$  and  $\theta_c$  were taken from Jordan's sounding, which has been used in many such studies (Ooyama 1969).

A typical run for which a hurricane life cycle was simulated by the model consisted of the following parameters:  $T_{\text{sea}} = 300.5 \text{ K}$ ,  $r_{v_{\text{max}}} = 90 \text{ km}$ , initial  $V_{\text{max}} = 11 \text{ m s}^{-1}$ . The variation

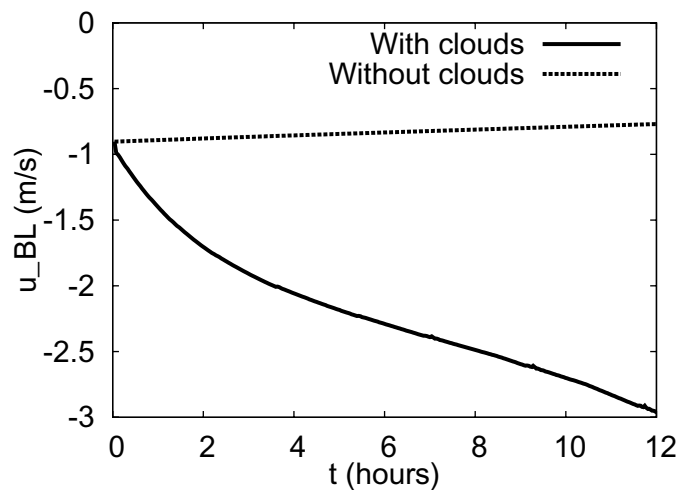


**Figure 3.** Radial flow in the boundary layer ( $u_{BL}$ ) with and without cloud heating as a function of time.

of the velocity field with time is shown in figure 2. Initially, the radius of maximum wind is 90 km. The initial wind is strong enough to cause large sea-surface fluxes. This leads to increased heating and updraft mass flux in the clouds. This increases the radial flow in the boundary layer, which increases the azimuthal velocity (the first term in equation (1)). There are two main effects of the cloud. One is in increasing  $u_{BL}$  and the other in lifting the streamlines (by vertical heating) and thus increasing the stretching. Initially, the streamlines consist of horizontal segments (inflow in the boundary layer and outflow at higher levels) connected by a curved section. As the vorticity intensifies, the vertical velocity gets established; with larger values away from the surface (mid-levels), streamlines get lifted up due to advection by the vertical velocity.

The time evolution of the radial inflow with and without the cloud heating term is shown in figure 3. Without clouds, the radial inflow decreases and approaches zero as the vortex decays. The effect of clouds is to increase the inflow, which in turn increases the vertical velocities.

Evolution of the heating rate due to clouds is shown in figure 4. One can see that the maxima move inwards and upwards as the time progresses. Also, the heating rates increase during the growth phase (48 h). The interaction between the azimuthal component of surface wind, sea-surface fluxes, cumulus heating at higher levels and secondary circulation constitutes a positive feedback cycle. Higher surface azimuthal winds ( $v$ ) increase the sea-surface fluxes, which in turn increase the cumulus heating at higher levels. This increases the secondary flow ( $u, w$ ), which leads to increased azimuthal winds.

As the vortex amplifies, the radius of maximum winds decreases. Velocities also increase at the upper levels by both diffusion and advection. This positive feedback leads to rapid amplification of the vortex (phase 1). The velocity reaches storm strength in 17 h and hurricane strength in 25 h. Then there is slowing down of the increase as the dissipative processes increase (phase 2). The velocity maxima are reached at 48 h. There is a balance of the tendencies to intensify and decay, so that near steady state is reached. Then there is the third phase that consists of a slow decay of the vortex. The rate of decay here is lower than that for the case with no clouds as the cloud heating opposes the decay.

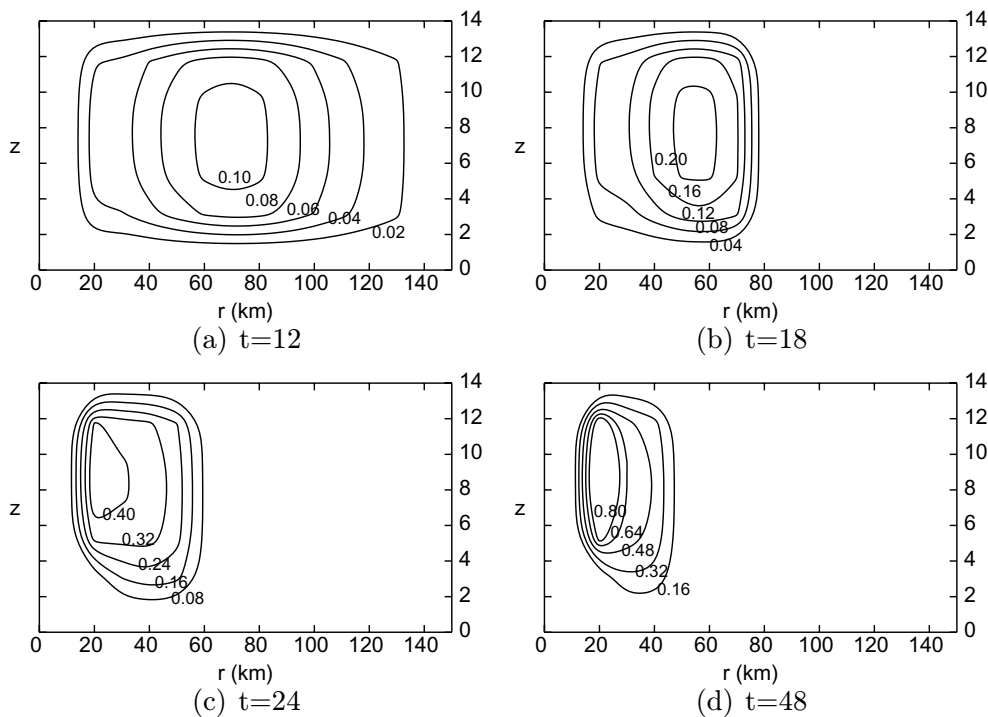


**Figure 4.** Cross sections of the heating rate for integration started with initial  $V_{\max} = 11 \text{ m s}^{-1}$  at (a)  $t = 12 \text{ h}$ , (b)  $t = 18 \text{ h}$ , (c)  $t = 24 \text{ h}$  and (d)  $t = 48 \text{ h}$ .

The structure of the vortex when maximum velocity is reached (48 h) is shown in figure 5. Contours of the azimuthal velocity  $v$  are shown in figure 5(a). The maxima close to the centre and the decrease both radially and in the vertical can be seen. From the plot of the streamfunction (figure 5(b)), the secondary circulation can be seen. The radial inflow in the boundary layer, large upward velocities in the central portion and radial outflow at higher levels can be seen. The high amounts of moisture in the boundary layer and regions of heating in the centre can be inferred from the contour plots of the saturated equivalent potential temperature  $\theta_e^*$  (figure 5(c)). The warm core structure of the vortex is clearly seen from figure 5(d), where the perturbation potential temperature ( $\theta'_v$ ) is plotted.

The radial profiles of azimuthal velocity are shown in figure 6. The growth is rapid with the maximum velocity increasing and the radius of maximum winds decreasing from 90 km initially to 20 km at 48 h. The variation is qualitatively similar to that simulated by Sundqvist's model. The time taken to reach the maximum velocity is longer though (84 h) in their case. In the decay phase, the shape of the radial profile is nearly the same.

#### 4.2. Finite amplitude nature

The finite-amplitude nature is evident on comparing simulations performed with different maximum initial velocities. The results are shown in table 4 and figure 7. In table 4,  $V_{\max}$  is the maximum velocity reached in the run,  $t_{V_{\max}}$  the time at which this velocity is reached,  $T_{\text{hurricane}}$  the duration for which  $v$  is above  $33 \text{ m s}^{-1}$  and  $T_{\text{storm}}$  the duration for which  $v$  is above  $17 \text{ m s}^{-1}$ . For a very weak vortex ( $V_0 = 2$ ), there is hardly any increase in the velocity. For  $V_0 = 5 \text{ m s}^{-1}$ , there is some amplification with a doubling of the initial strength

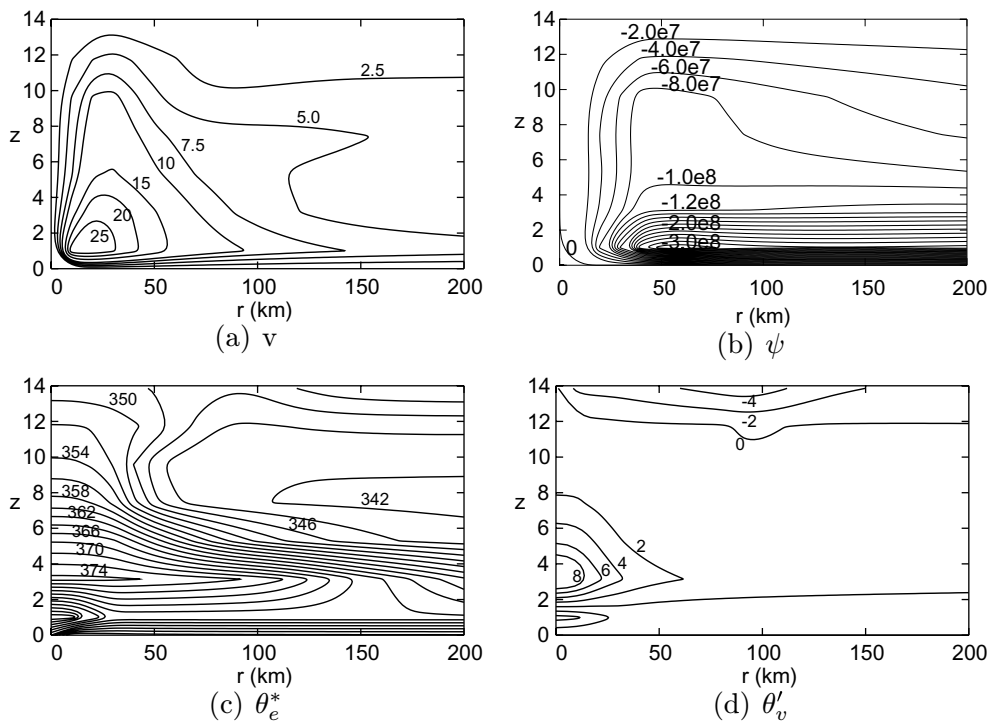


**Figure 5.** Structure of the vortex at  $t = 48$  h for integration started with initial  $V_{\max} = 11 \text{ m s}^{-1}$ . In the  $r$ - $z$  plane, contours are plotted for the following fields: (a) azimuthal velocity  $v$  ( $\text{m s}^{-1}$ ), (b) streamfunction, (c) saturated equivalent potential temperature  $\theta_e^*$  (K) and (d) perturbation potential temperature  $\theta'_v$  (K).

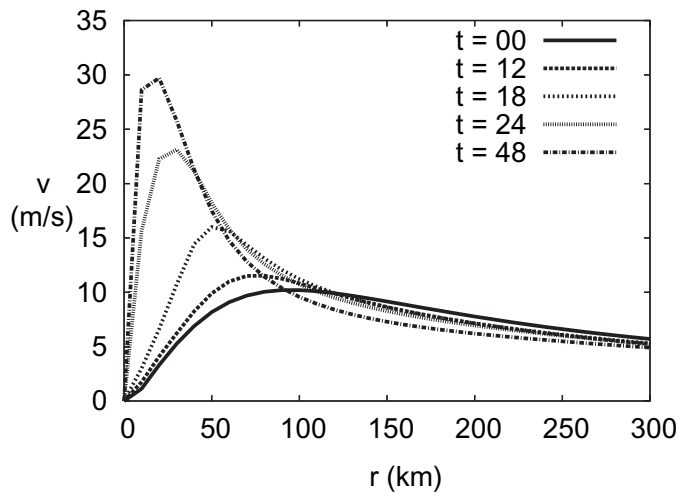


**Figure 6.** Evolution of the vortex with an initial maximum velocity of  $11 \text{ m s}^{-1}$ . Radial distribution of azimuthal velocity is plotted at different times (in hours).

by 86 h, followed by a decay. For  $V_0 = 8 \text{ m s}^{-1}$ , more rapid intensification takes place and tropical storm strength is reached within 2 days, a maximum velocity of  $24 \text{ m s}^{-1}$  in 64 h, followed by a slow decay. For  $V_0 = 10 \text{ m s}^{-1}$  the behaviour is similar in structure to that

**Table 4.** Effect of initial vortex strength on the evolution of the system.  $V_{\max}$  is the maximum velocity reached in the run,  $t_{V_{\max}}$  the time at which this velocity is reached,  $T_{\text{hurricane}}$  the duration for which  $v$  is above  $33 \text{ m s}^{-1}$  and  $T_{\text{storm}}$  the duration for which  $v$  is above  $17 \text{ m s}^{-1}$ .

$V_0$ ( $\text{m s}^{-1}$ )	$V_{\max}$ ( $\text{m s}^{-1}$ )	$t_{V_{\max}}$ (h)	$T_{\text{hurricane}}$ (h)	$T_{\text{storm}}$ (h)
2.0	2.01	34.42	–	–
5.0	11.98	86.63	–	–
8.0	23.93	64.02	–	132
10.0	32.93	49.87	–	220
11.0	37.32	48.01	78	224
12.0	41.90	48.01	118	227

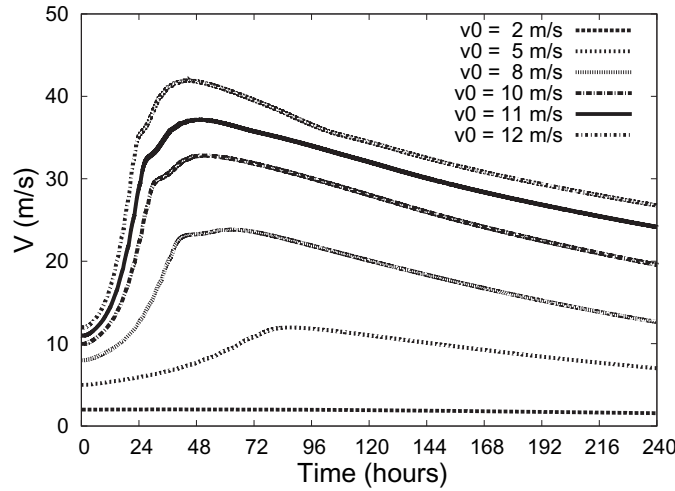


**Figure 7.** Evolution of full vortices of different initial strengths ( $v_0$ ) is shown by plotting the maximum azimuthal velocity ( $v$ ) with time.

with  $V_0 = 11 \text{ m s}^{-1}$ , except that the maximum velocity just reaches the hurricane strength of  $33 \text{ m s}^{-1}$ . For  $V_0 = 12 \text{ m s}^{-1}$ , the maximum velocity reached is  $41.90 \text{ m s}^{-1}$  and the hurricane is sustained for nearly 5 days. The finite amplitude effect observed in these simulations is similar to the results of Rotunno and Emanuel (1986) and Emanuel (1989).

The maximum potential intensity (MPI) theory of Emanuel (1988) and Holland (1997) provides a limit on the strength of a hurricane based on the environmental factors such as ambient humidity and SST. We found that the maximum strength reached in the simulations is lower than the value from MPI for similar ambient conditions. For example, for  $T_{\text{sea}} = 300.5 \text{ K}$ , a  $V_{\max}$  of  $45.97 \text{ m s}^{-1}$  is predicted by MPI, while our calculation is  $41.90$  for an initial vortex strength of  $12$  (table 4).

The reason for the finite amplitude nature can be understood as follows. In figure 8, the evolutions of the individual terms (denoted by T1, T2 and T3) on the rhs of equation (1), at a point close to the maxima of azimuthal velocity, for various values of the initial vortex strengths are compared. At this point, T1 ( $-u\eta$ ) and T3 ( $D_v$ ) are negative for the most part, while T2 ( $-w\partial v/\partial z$ ) is positive. Vortex amplification is due to T2, which is mainly due to the induced vertical velocity. This tendency is opposed by terms T2, radial advection, and T3, the turbulent diffusion term. The relative magnitude of T2 with respect to T1 and T3 determines

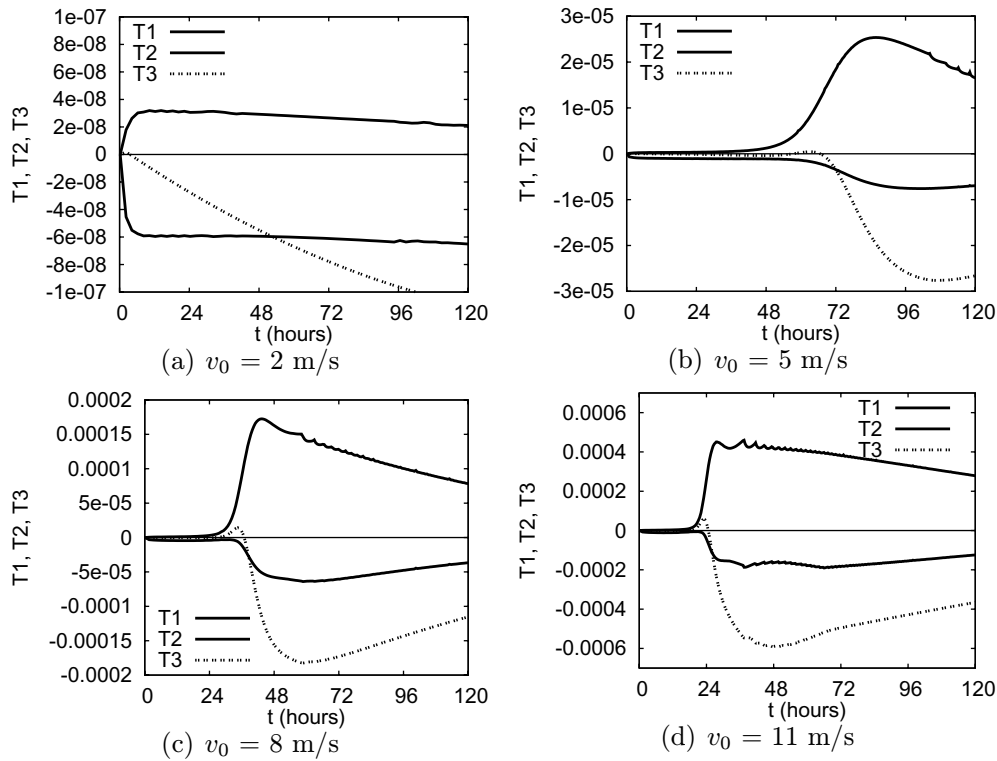


**Figure 8.** Evolution of the terms (T1, T2 and T3) on the rhs of equation (1), at a point close to the maxima of azimuthal velocity, for full vortices of different initial strengths.

whether amplification or decay occurs. For small initial velocities ( $v_0 = 2 \text{ m s}^{-1}$ , figure 8(a)), T1 dominates T2 and therefore there is only decay of the vortex.

For intermediate velocities ( $v_0 = 5 \text{ m s}^{-1}$ , figure 8(b)), after about 24 h, T2 increases rapidly, since the radial inflow in the boundary layer is of sufficient strength to higher vertical velocities at higher levels. The corresponding increase in T1 is not sufficient. It takes some time for T3 to increase and arrest further growth of the vortex, so only a moderate strength is reached followed by a decay phase.

For velocities above a threshold ( $v_0 = 8, 11 \text{ m s}^{-1}$ , figures 8(c) and (d)), the radial inflow in the boundary layer, and the corresponding induced vertical velocities at higher levels close to the centre of the vortex, is sufficiently high and T2 increases exponentially. There is a lag of around 12 h for T3 to increase. Then quasi-equilibrium is reached before T3 dominates and causes the vortex to decay.

#### 4.3. Parameter sweep experiments

The effect of various parameters on the formation is described below. For these comparisons, the case with  $V_0 = 11$  was chosen as the control run.

On doubling the domain, keeping the grid size the same, the change in the maximum velocity is marginal (from 32.93 to 33.42). This shows that the domain of 500 km is adequate for the present study.

**Table 5.** Effect of the initial radius of maximum winds ( $r_{v_{\max}}$ ) on the evolution of the system.

$r_{v_{\max}}$ (km)	50	60	70	80	90	100	125	150
$V_{\max}$ ( $\text{m s}^{-1}$ )	24.20	27.75	31.19	34.16	37.32	39.84	45.92	50.92

**Table 6.** Effect of SST on the evolution of the system.

$T_{\text{sea}}$ (K)	298.5	299.0	299.5	300.0	300.5	301.0	301.5	302.0	302.5
$V_{\max}$ ( $\text{m s}^{-1}$ )	30.18	30.97	33.13	35.24	37.19	40.01	43.40	46.96	48.73

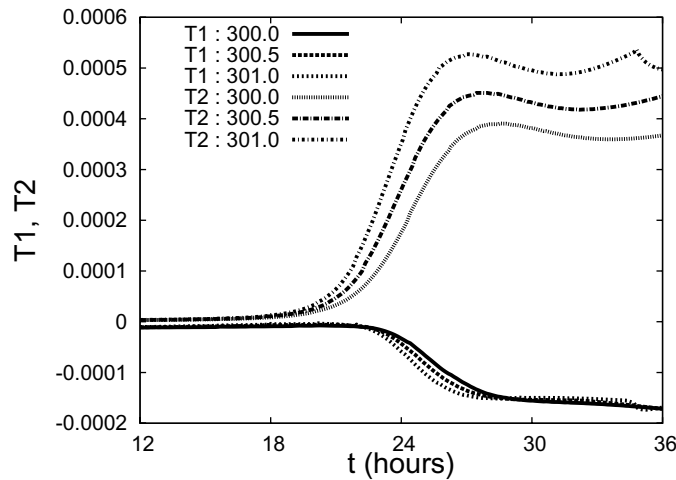


**Figure 9.** Evolution of the terms T1 and T2 on the rhs of equation (1) for full vortices when the SST is varied.

If the radius of maximum wind is decreased from 100 to 50 km, (a change of 50%), the maximum wind decreases from 39.84 to 24.20  $\text{m s}^{-1}$  (a change of 39.3%) (table 5). The reduction is due to the reduced strength of the initial vortex. If the radius of maximum wind is increased to 150 km (a change of 50%), the maximum wind increases to 50.92 (a change of 27.8%). The percentage decrease/increase is lower than that of the change in  $r_{v_{\max}}$ . This suggests that this parameter has a moderate impact.

Amplification depends more on the initial velocity, as seen from table 4 and figure 7. If both the velocity and the radius of maximum wind are varied keeping the vorticity constant, the behaviour is similar to that seen in table 4.

The variation of the maximum velocity reached when the sea-surface temperature is varied is shown in table 6. The nonlinear nature of the effect of SST can be seen. A decrease of 2 K results in a decrease  $V_{\max}$  of around 7  $\text{m s}^{-1}$ , while an increase of 2 K results in an increase  $V_{\max}$  of around 11.5  $\text{m s}^{-1}$ . When SST is changed, the major impact is on the vertical velocities (the term T2), while the radial flow (the term T1) is affected marginally (figure 9). The changes in vertical velocity are in turn due to reduction/increase of fluxes from the sea. This is to be expected as the heating is linked to the sea-surface fluxes in our formulation of the model. The large percentage change shows that this is an important parameter.

The effect of the Coriolis parameter was studied by varying the base latitude as given in table 3. The maximum values of  $v$  reached are shown in table 7. The general trend (from 17°N) is that  $v_{\max}$  decreases with increasing latitude. This is because an increase in the value

**Table 7.** Effect of the Coriolis parameter on the evolution of the system.

Latitude ( $^{\circ}$ N)	15	16	17	18	19	20	22.5	25
$V_{\max}$ ( $\text{m s}^{-1}$ )	39.27 <sup>a</sup>	41.85 <sup>a</sup>	42.17	39.89	38.86	37.19	34.96	33.03

<sup>a</sup> Oscillations are observed.

**Table 8.** Effect of the Coriolis parameter on the evolution of the system, with an increased value of the eddy viscosity parameter:  $l_h = 2400$ .

Latitude ( $^{\circ}$ N)	15	16	17	18	19	20	22.5	25
$V_{\max}$ ( $\text{m s}^{-1}$ )	33.03	32.75	31.05	29.97	29.21	28.59	26.91	25.82

of  $f$  leads to an increase in the term T2, which tends to oppose the amplification of the vortex. For latitudes  $15^{\circ}$ N and  $16^{\circ}$ N, large fluctuations are observed in the velocity versus time graph. Decreasing the time step did not change the results, indicating that this was not a problem of numerical stability. The decrease of inertial stability when the Coriolis parameter is reduced could be the cause. Most other studies like those of Emanuel, Sundqvist and Zhu *et al* have used the  $20^{\circ}$ N as the base latitude, probably for this reason. As a further check, the horizontal eddy viscosity term ( $K_H$ ) was increased by increasing  $l_h$  from 2000 to 2400. This led to a suppression of the oscillations and a decrease in the maximum velocity reached (from 39.27 to 33.03). With this higher value of  $l_h$ , the  $V_{\max}$  decreases monotonically as latitude increases (table 8).

#### 4.4. Mid-level vortices

The mechanism for the formation of mid-level vortices is well known and can be explained by the thermal wind relation (Raymond and Jiang 1990). In a region of the tropics having a large cumulus cloud, stratiform heating takes place in the anvil region due to the release of latent heat of condensation. If the region is not saturated, there is re-evaporation of rain in the lower troposphere, causing it to cool. Thus a vertical dipole of heating is formed. If this heating pattern is sustained and if the local Rossby radius of deformation is reduced, it results in temperature perturbations having nearly the same spatial pattern. Thermal wind balance then requires the formation of a mid-level vortex. This process is simulated by specifying the heating pattern by the function  $\dot{Q}(r, z) = -\sin(2\pi z/z_{\max}) \exp(-\alpha r^2)$ . The resulting velocity field has a maximum in the middle of the domain ( $z_{\max}/2$ ).

**4.4.1. Decay of mid-level vortices.** To demonstrate the decay of mid-level vortices, simulations were performed keeping all the other parameters the same as in the previous study but changing the initial condition to that for a mid-level vortex. In the vertical, the velocity maximum was chosen to be at levels 4 and 5. Above and below this level, the variation of velocity was taken to be  $(1/2)(1.0 + \tanh(3(z_c - 1/2)))$ , where  $z_c$  is the vertical distance measured from this level, normalized by the vertical distance to the domain limits (boundary layer height below and  $z_{\max}$  above).

The main forcing here is that due to turbulent dissipation, which is weak at mid-levels because no surface processes are present. In the model, the minimum values of the eddy viscosities were set as  $1 \text{ m}^2 \text{ s}^{-1}$  in the vertical direction and  $100 \text{ m}^2 \text{ s}^{-1}$  in the radial direction. This led to a very slow spin-down. The results are shown in figure 10. For the same vortex strengths, which caused hurricane formation when placed just above the boundary layer, there is either slow decay ( $V_0 = 10$ ) or marginal increase ( $V_0 = 12$ ). There is slow diffusion of the

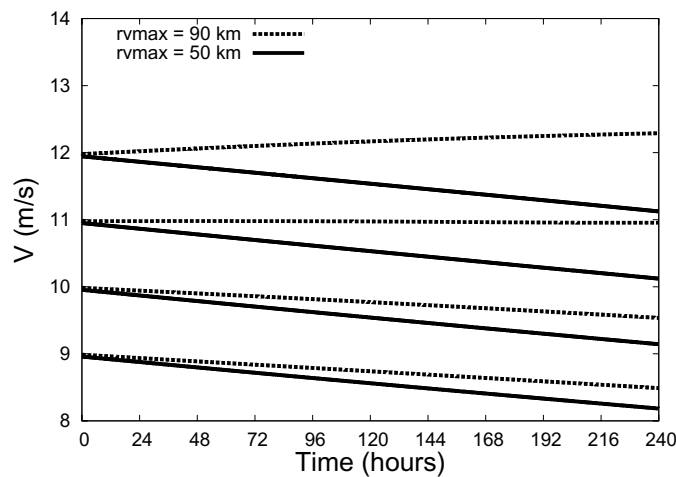


**Figure 10.** Evolution of mid-level vortices of different initial strengths ( $v_0$ ) and the location of the radius of maximum winds ( $r_{v_{\max}}$ ) are shown by plotting the maximum azimuthal velocity ( $v$ ) against time.

vorticity causing the surface vortex to grow, but the magnitude reached even after 10 days is too small for convection to be triggered. Thus, for all practical purposes, the vorticity can be considered constant.

**4.4.2. Extension to the boundary layer:** The present model, being an axisymmetric one, cannot simulate the baroclinic, three-dimensional merger of two mid-level vortices. We use the results available in the literature for this problem and study the evolution following a merger by introducing a suitable ‘merged’ vortex. The ‘merged vortex’ is simulated by specifying a mid-level vortex with increased vertical extent. This is due to the existence of an optimum aspect ratio as shown by studies of Reinaud *et al* (2003).

We construct ‘merged’ mesoscale vortices by stretching the vertical profile of velocity. The velocities of the level of maximum velocity and the levels above are left untouched. Each level below is assigned the value of the level above it (of the original profile). The reason for this is that in the simulations of merger of mid-level vortices (Ritchie and Holland 1997), the increase in the vertical direction is mainly below the initial vortex. The increase above is marginal.

While considering mid-level vortices, there are two possibilities: (i) only a mid-level vortex is present with no surface vorticity and (ii) a weak surface vortex is present along with the merged mid-level vortices. Ritchie and Holland (1997) have shown that the presence of a surface vortex typical of a monsoon trough enhances the merger process. This was demonstrated also by vortex patch simulations, where presence of a large-scale depression results in an increase in the distances up to which merger takes place (Venkatesh 2003). Montgomery and Enagonio (1998) simulated a mid-level vortex with peripheral convection and showed that the axisymmetrization process leads to a spin-up of a surface vortex. Therefore, simulations were performed for both the cases.

For the second case, an additional surface vortex obtained by extending the tanh velocity profile to the top of the boundary layer was used. The strength of the surface vortex was varied from  $2.4 \times 10^{-5}$  to  $2.2 \times 10^{-4}$ . These values are comparable with the value ( $23 \times 10^{-5} \text{ s}^{-1}$ ) taken by Ritchie and Holland (1997). The results for both the cases are as follows.

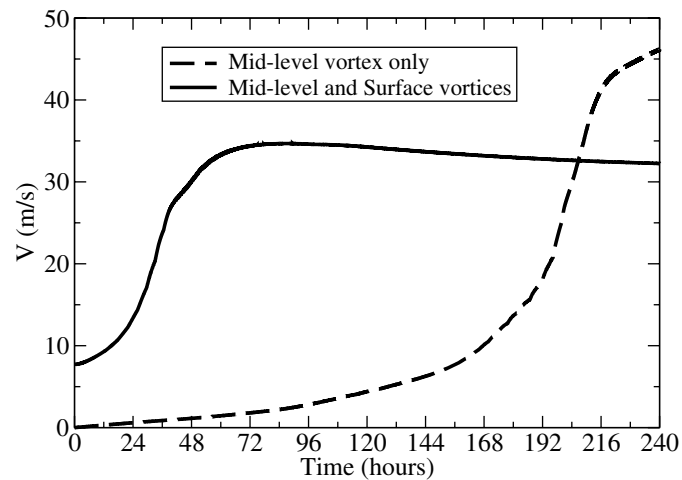


**Figure 11.** Evolution of the maximum azimuthal surface wind ( $\text{m s}^{-1}$ ) is shown when (a) only a mid-level vortex is present (dashed line) and (b) a mid-level vortex and a surface vortex are present (solid line). The initial strengths of the mid-level and surface vortices are  $V_{\text{max}} = 12$  and  $7 \text{ m s}^{-1}$ , respectively.

#### *Without a surface vortex*

For both the half extended case (stretching of velocity profile by one level) and extended case (stretching of velocity profile by two levels), with the surface velocity set as zero, the overall behaviour is identical. The reason for this is that vertical diffusion makes the velocity profiles below the vortex reach a similar state in a very short time for both the cases. The subsequent development is then identical. Initially, the mid-level vortex decays slowly and the surface vorticity grows. By 100 h, the surface vortex is strong enough for surface fluxes and convection to develop. Then there is rapid growth of the surface vorticity and reduction of the mid-level vorticity (due to eddy diffusion). By 150 h, the surface vortex becomes stronger and intensifies, reaching hurricane intensity by 200 h (figure 11). In reality, it is unlikely that this sequence of events would occur, as the time taken for the surface vortex to amplify (100 h) is too large. The chief effect of mean winds, which cannot be accounted for in the present model, would be to advect the mid-level vortices over a period of 4–5 days. In simulations by Rogers and Fritsch (2001), the time for vorticity to reach the surface is of the order of a few hours.

#### *With a surface vortex*

The time evolution of velocity for this case is when the surface vorticity is  $17 \times 10^{-5}$  as is shown in figure 11. The surface vortex initiates convection and grows rapidly, overtaking the mid-level vortex within a day. It intensifies to hurricane strengths in 60 h and a maximum velocity of  $35 \text{ m s}^{-1}$  is reached by 75 h, followed by a gradual decay. The structure of the vortex at steady state is similar to that obtained from the amplification of a full vortex. It should be noted that a full vortex with  $V_0 = 8 \text{ m s}^{-1}$  does not intensify into a hurricane. The evolution in this case is closer to that of the full vortex with  $V_0 = 12 \text{ m s}^{-1}$ . Furthermore, there is a longer quasi-steady state.

The strength of the surface vortex determines the time taken for amplification (see table 9). For weak surface vortices, the time needed to reach hurricane strength is more than

**Table 9.** Effect of the strength of the surface vortex on the time taken to reach hurricane strength.

Surface vorticity ( $\times 10^{-5} \text{ s}^{-1}$ )	2.4	4.8	7.3	9.7	12.2	14.6	17.0	19.5	22.0
$t_{\text{hurr}}$ (h)	178	142	123	112	115	83	60	42	31

5 days. For vortices with strength  $17 \times 10^{-5} \text{ s}^{-1}$  or greater, the timescale of amplification is realistic.

## 5. Summary and conclusions

A simple axisymmetric model has been developed for tropical cyclone-related studies. A feature of this model is that it can resolve the vertical structure of vortices that are likely to be present in the early stages of genesis. The model numerics has been validated using the analytical results available for spin-down half-lives. For full vortices, studies of the finite amplitude nature and the dependence on various parameters, like the sea-surface temperature, Coriolis parameter and initial vortex strength, have been carried out and these compare well with other simulations of this kind.

The main results of the balanced vortex calculations are the following: If no cloud heating is present, full vortices decay in about 5 days with the decay rate increasing with the initial strength. Mid-level vortices, on the other hand, decay very slowly and can be assumed to remain nearly steady. With cloud heating and sea-surface fluxes, full vortices amplify, reach hurricane strength within 2 days, are in a quasi-steady state for around 4–5 days and decay slowly. The finite amplitude nature of this amplification is also evident. While weak vortices decay, those above a threshold ( $V_0 = 10 \text{ m s}^{-1}$ ,  $r_{v_{\text{max}}} = 90 \text{ km}$ ) amplify. The maximum velocity reached and the duration of the hurricane depend on the initial velocity. The sea-surface temperature has a crucial role, and the maximum velocity reached depends on small changes to it.

Merged mid-level vortices with an increased vertical extent but with no vorticity at the surface amplify but not on a realistic time-scale. Merged mid-level vortices with an increased vertical extent and with a surface depression of typical strength amplify and reach hurricane strengths.

A novel feature of this paper is that a comparison of the evolution of mid-level vortices and full vortices was done. It is shown that mid-level vortices decay if no other effects are present. Also it is shown that if merger is simulated and the strength of the surface vortex increases, there is a rapid intensification of these vortices, in a manner similar to full vortices. These results form an important part of the evidence in favour of the authors' model (Venkatesh and Mathew 2004) for tropical cyclone genesis.

## References

- Bister M and Emanuel K A 1997 The genesis of Hurricane Guillermo: TEXMEX analyses and a modeling study *Mon. Weather Rev.* **125** 2662–82
- Challa M and Pfeffer R L 1980 Effects of eddy fluxes of angular momentum on the model hurricane development *J. Atmos. Sci.* **37** 1603–18
- Challa M, Pfeffer R L, Zhao Q and Chang S W 1998 Can eddy fluxes serve as a catalyst for Hurricane and Typhoon formation? *J. Atmos. Sci.* **55** 2201–19
- Eliassen A 1952 Slow thermally or frictionally controlled meridional circulation in a circular vortex *Astrophys. Norveg.* **5** 19–60

- Eliassen A and Lystad M 1977 The Ekman layer of a circular vortex. A numerical and theoretical study *Geophys. Norveg.* **31** 1–16
- Emanuel K A 1986 An air–sea interaction theory for tropical cyclones. Part I: Steady state maintenance *J. Atmos. Sci.* **43** 585–604
- Emanuel K A 1988 The maximum intensity of hurricanes *J. Atmos. Sci.* **45** 1143–55
- Emanuel K A 1989 Finite amplitude nature of tropical cyclogenesis *J. Atmos. Sci.* **46** 3431–56
- Emanuel K A 1995 The behavior of a simple hurricane model using a convective scheme based on subcloud layer entropy equilibrium *J. Atmos. Sci.* **52** 3960–8
- Fudeyasu H, Wang Y, Satoh M, Nasuno T, Miura H and Yanase W 2008 Global cloud-system-resolving model NICAM successfully simulated the lifecycles of two real tropical cyclones *Geophys. Res. Lett.* **35** L22808
- Hendricks E A, Montgomery M T and Davis C A 2004 The role of ‘vortical’ hot towers in the formation of tropical cyclone Diana (1984) *J. Atmos. Sci.* **61** 1209
- Holland G J 1997 The maximum potential intensity of tropical cyclones *J. Atmos. Sci.* **54** 2519–41
- Houze R A 1993 *Cloud Dynamics* (New York: Academic)
- Jordan C L 1958 Mean soundings for the West Indies area *J. Meteorol.* **15** 91–7
- Khalili A, Basu A J and Mathew J 1997 A simpler implicit scheme for computing unsteady incompressible flows *Comput. Fluid Dyn. J.* **6** 385–98
- Kim J and Moin P 1985 Application of a fractional step method to incompressible Navier–Stokes equations *J. Comput. Phys.* **59** 308–23
- Montgomery M T and Enagonio J 1998 Tropical cyclogenesis via convectively forced vortex Rossby waves in a 3-D quasi-geostrophic model *J. Atmos. Sci.* **55** 3176–207
- Montgomery M T, Snell H D and Yang Z 2001 Axisymmetric spindown of dynamics of hurricane-like vortices *J. Atmos. Sci.* **58** 421–35
- Montgomery M T, Nicholls M E, Cram T A and Saunders A B 2006 A vortical hot tower route to tropical cyclogenesis *J. Atmos. Sci.* **63** 355–86
- Ooyama K 1969 Numerical simulation of the life cycle of tropical cyclones *J. Atmos. Sci.* **26** 3–40
- Raymond D J and Jiang H 1990 A theory for long-lived mesoscale convective systems *J. Atmos. Sci.* **47** 3067–77
- Reinaud J N, Dritschel D G and Koudella C R 2003 The shape of vortices in quasi-geostrophic turbulence *J. Fluid Mech.* **474** 175–92
- Ritchie E A and Holland G J 1997 Scale interactions during the formation of typhoon Irving *Mon. Weather Rev.* **125** 1377–96
- Rogers R F and Fritsch J M 2001 Surface cyclogenesis from convectively driven amplification of midlevel convective vortices *Mon. Weather Rev.* **129** 605–37
- Rotunno R and Emanuel K A 1987 An air–sea interaction theory for tropical cyclones. Part II: Evolutionary study using a nonhydrostatic axisymmetric numerical model *J. Atmos. Sci.* **44** 542–61
- Schubert W H and Hack J J 1982 Inertial stability and tropical cyclone development *J. Atmos. Sci.* **39** 1687–97
- Schubert W H and Hack J J 1983 Transformed Eliassen balanced vortex model *J. Atmos. Sci.* **40** 1571–83
- Sundqvist H 1970 Numerical simulation of the development of tropical cyclones with a ten level model *Tellus* **22** 359–90
- Venkatesh T N 2003 A vortex merger theory for tropical cyclone genesis *PhD Thesis* Department of Aerospace Engineering Indian Institute of Science, Bangalore, India
- Venkatesh T N 2006 Mesoscale interactions during the genesis and intensification of the 1999 Orissa supercyclone *Mausam* **57** 31–6
- Venkatesh T N and Mathew J 2004 Prediction of tropical cyclone genesis using a vortex merger index *Geophys. Res. Lett.* **31** L04105
- Wirth V 1998 Thermally forced stationary axisymmetric flow on the  $f$ -plane in a nearly frictionless atmosphere *J. Atmos. Sci.* **55** 3024–41
- Zhu H and Smith R K 2002 The importance of three physical processes in a minimal three dimensional tropical cyclone model *J. Atmos. Sci.* **59** 1825–40
- Zhu H, Smith R K and Ulrich W 2001 A minimal three dimensional tropical cyclone model *J. Atmos. Sci.* **58** 1924–43